Journal of Controlled Release 324 (2020) 586–597

Contents lists available at ScienceDirect

Journal of Controlled Release

journal homepage: www.elsevier.com/locate/jconrel

Endosome-triggered ion-releasing nanoparticles as therapeutics to enhance the angiogenic efficacy of human mesenchymal stem cells

Gwang-Bum Im[a,1], Euiyoung Jung[b,c,1], Yeong Hwan Kim[a], Yu-Jin Kim[a], Sung-Won Kim[a], Gun-Jae Jeong[d], Tae-Jin Lee[a,e], Dong-Ik Kim[d], Jinheung Kim[c], Taeghwan Hyeon[f,g], Taekyung Yu[b,*], Suk Ho Bhang[a,*]

[a] School of Chemical Engineering, Sungkyunkwan University, Suwon 16419, Republic of Korea
[b] Department of Chemical Engineering, Kyung Hee University, Youngin 17104, Republic of Korea
[c] Department of Chemistry and Nano Science, Ewha Womans University, Seoul 120-750, Republic of Korea
[d] Division of Vascular Surgery, Samsung Medical Center, Sungkyunkwan University School of Medicine, Seoul 06351, Republic of Korea
[e] Department of Medical Biotechnology, Division of Medical Biotechnology, College of Biomedical Science, Kangwon National University, Chuncheon-si, Gangwon-do, 24341, Republic of Korea
[f] Center for Nanoparticle Research, Institute for Basic Science (IBS), Seoul 08826, Republic of Korea
[g] School of Chemical and Biological Engineering, Institute of Chemical Process, Seoul National University, Seoul 08826, Republic of Korea

ARTICLE INFO

Keywords:
Angiogenesis
Cell homing
Endosome-triggered nanoparticles
Intracellular ROS control
Stem cell

ABSTRACT

Here, we report that Fe ions delivered into human mesenchymal stem cells (hMSCs) by bioreducible metal nanoparticles (NPs) enhance their angiogenic and cell-homing efficacy by controlling ion-triggered intracellular reactive oxygen species (ROS) and improve cell migration, while reducing cytotoxicity. Endosome-triggered iron-ion-releasing nanoparticles (ETIN) were designed to be low-pH responsive to take advantage of the low-pH conditions (4–5) of endosomes for *in situ* iron-ion release. Due to the different redox potentials of Fe and Au, only Fe could be ionized and released from our novel ETIN, while Au remained intact after ETIN endocytosis. Treatment with an optimal amount of ETIN led to a mild increase in intracellular ROS levels in hMSCs, which enhanced the expression of HIF-1α, a key trigger for angiogenic growth factor secretion from hMSCs. Treatmetn of hMSCs with ETIN significantly enhanced the expression of angiogenesis- and lesion-targeting-related genes and proteins. Transplantation of ETIN-treated hMSCs significantly enhanced angiogenesis and tissue regeneration in a wound-closing mouse model compared with those in untreated mice and mice that underwent conventional hMSC transplantation.

1. Introduction

Nanoparticles (NPs) offer major advantages to the biomedical field but also pose considerable challenges for clinical application. Studies have shown that NPs with diverse nanostructures and compositions have potential for versatile application in gene delivery [1], drug delivery [2], and theragnosis [3]. The advantages of NPs include their large surface area, controllable structures, and diverse surface chemistry [4,5]. Most studies on NPs have focused on the controlled release of genes or drugs [1,2], ease of entry into cells for efficient drug delivery [6], and enhanced specific cell and tissue targeting efficiency for reliable theragnosis [7]. However, the biodegradability of NPs must be researched to avoid unfavorable accumulation of NPs within the body as this can cause side effects such as inflammation and genetic mutation [8,9].

NPs can act as therapeutic agents by releasing specific metal ions into cells. Mesenchymal stem cell (MSC)-based therapies are a major focus of regenerative medicine, which is concerned with treating various inflammatory, ischemic, and neurologic diseases. The advantages of MSCs for cell therapy rely on their capacity to migrate toward a lesion and secrete various paracrine factors for tissue regeneration. The interaction between stromal cell-derived factor 1 alpha and its receptor C-X-C chemokine receptor type 4 (CXCR4) has been reported to be critical for regulating MSC migration [10]. A study suggested that CXCR4 overexpression is induced by Fe ions [11]. However, Fe ions are severely cytotoxic at high concentrations because of the oxidative stress

* Corresponding authors.
E-mail addresses: tkyu@khu.ac.kr (T. Yu), sukhobhang@skku.edu (S.H. Bhang).
[1] These authors contributed equally to this work.

https://doi.org/10.1016/j.jconrel.2020.05.038
Received 17 February 2020; Received in revised form 20 May 2020; Accepted 22 May 2020
Available online 23 May 2020
0168-3659/

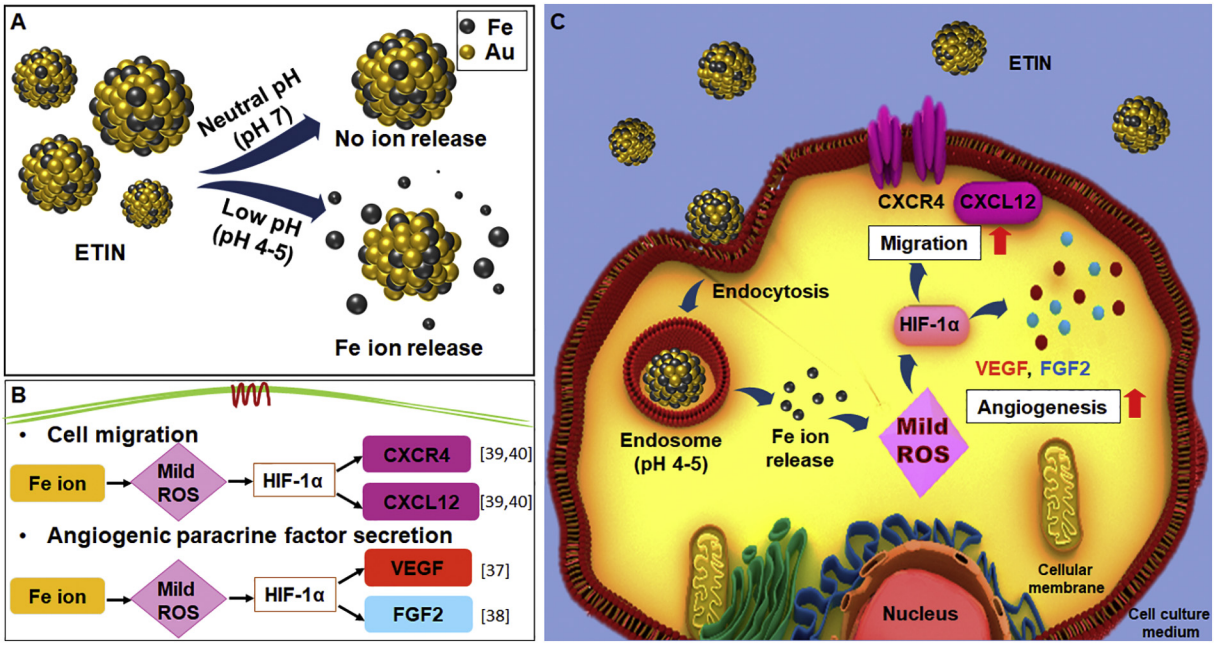

Scheme 1. Schematic of (A) ETIN that can release Fe ions in a pH-dependent manner and (B) the molecular mechanisms underlying the enhanced cell migration and secretion of angiogenic growth factors induced by intracellular Fe-ion release and mild ROS generation. (C) Intracellular delivery of pH-sensitive ETIN for Fe-ion delivery to enhance the therapeutic angiogenic effect of hMSCs. Abbreviation: ETIN, endosome-triggered iron-ion-releasing nanoparticles; ROS, reactive oxygen species; HIF-1α, hypoxia-inducible factor-1 alpha; CXCR4, C-X-C chemokine receptor type 4; CXCL12, C-X-C motif chemokine 12; VEGF, vascular endothelial growth factor; FGF2, fibroblast growth factor2.

that they can cause at such concentrations [12]. Therefore, the intracellular delivery of Fe ions may lead to beneficial biological effects such as cell migration and gene expression, without inducing cytotoxicity in MSCs. Thus, it may be feasible to use Fe-based bioreducible NPs to enhance the therapeutic efficacy of MSCs.

In this study, novel bioreducible endosome-triggered iron-ion-releasing nanoparticle (ETIN) were applied as a therapeutic substance for the delivery of metal (Fe) ions to enhance human mesenchymal stem cell (hMSC)-based wound healing. We designed the NPs such that Fe ions could be released within the cells in response to the low-pH conditions in endosomes. There are clear differences in the redox potentials and chemical reactivities of Fe and Au; Fe has a comparatively low standard redox potential in comparison with that of Au, which has a high standard redox potential [13]. Fe can promptly react with hydrogen ions and forms Fe ions under low-pH conditions, while Au does not react with hydrogen ions [14,15]. Therefore, the low-pH conditions (4–5) of endosomes can trigger the *in situ* release of Fe ions by degradation of ETIN after endocytosis (Scheme 1), while Au remains unaffected. In this study, Au was selected to synthesize the Fe-ion releasing NPs because Au is non-toxic and non-degradable and can be used for tracking ETIN after endocytosis. Furthermore, a simple surface modification of Au may provide more functions to the ETIN, such as gene delivery and bioimaging, in addition to intracellular Fe-ion delivery.

2. Results

2.1. Characterization of ETIN

Transmission electron microscopy (TEM) images of the ETIN (Fig. 1A) showed spherical nanoparticles with an average size of 3.4 ± 0.4 nm (Fig. 1B). The high-resolution TEM images of a single ETIN demonstrated that the NP has a single-crystalline nature (Fig. 1A). All the ETIN X-ray powder diffraction (XRD) peaks were shifted to slightly higher angles, compared with the XRD peaks for pure Au NPs (Fm3m, a = 4.078 Å, Joint Committee on Powder Diffraction Standards [JCPDS] file No. 04–0784) due to the smaller size of the Fe atom compared with that of the Au atom (Fig. 1C). The UV–Vis spectra of the ETIN showed the presence of a plasmon resonance peak at 520 nm (Fig. 1D), revealing a slight red shift, compared with the spectra of pure Au NPs [16]. We investigated Fe-ion release from ETIN at an acidic condition (pH 4.5). A red-shifted absorption peak was observed in the UV–vis spectrum under the acidic condition, whereas no change was observed for the neutral condition (pH 7.0, Fig. 1D). The UV–vis results showed that Fe ions were released from the ETIN under endosome-mimicking conditions. The amount of released Fe ions under acidic relative to that released under neutral pH conditions (4.5 and 7.0) was evaluated by energy dispersive spectrometry (EDS) (Fig. 1E). The Au/Fe atomic ratio under acidic conditions was approximately 3-fold higher than that under neutral conditions. ETIN distributed in deionized (DI) water, which served as the standard condition (pH 7–8), showed no significant difference in the Au/Fe atomic ratio from that under neutral conditions (Fig. 1E). The EDS profiles clearly showed that the ETIN only comprised Au and Fe (Figs. 1F and S1). As shown in Fig. 1H, water-based ETIN were synthesized by simultaneously adding $HAuCl_4$ and $FeCl_3$ solutions to poly(vinyl pyrrolidone) (PVP) and stirring the mixture at 600 rpm for 15 min at room temperature (RT). We thus synthesized novel ETIN that can release Fe ions in a pH-dependent manner. TEM and EDS mapping images of ETINs stored for 6 months at 4 °C showed long-term stability, with uniform size, shape, and composition (Fig. S1).

2.2. Cytotoxicity test of ETIN

Iron ions released from ETIN induced mild ROS generation in hMSCs, which can affect the cellular microenvironment (Fig. 2A and B). Severe ROS generation inside cells is known to upregulate the expression of apoptotic genes, such as *BAX* and *CASPASE-3* [17]. In this study, more than 25 μg/mL ETIN significantly increased *BAX* and *CASPASE-3* expression (Fig. 2C and D). To confirm the cytotoxic effect of ETIN on hMSCs, cell viability was evaluated by CCK-8 analysis. Cell viability 24 h after treatment with ETIN was not significantly different from that

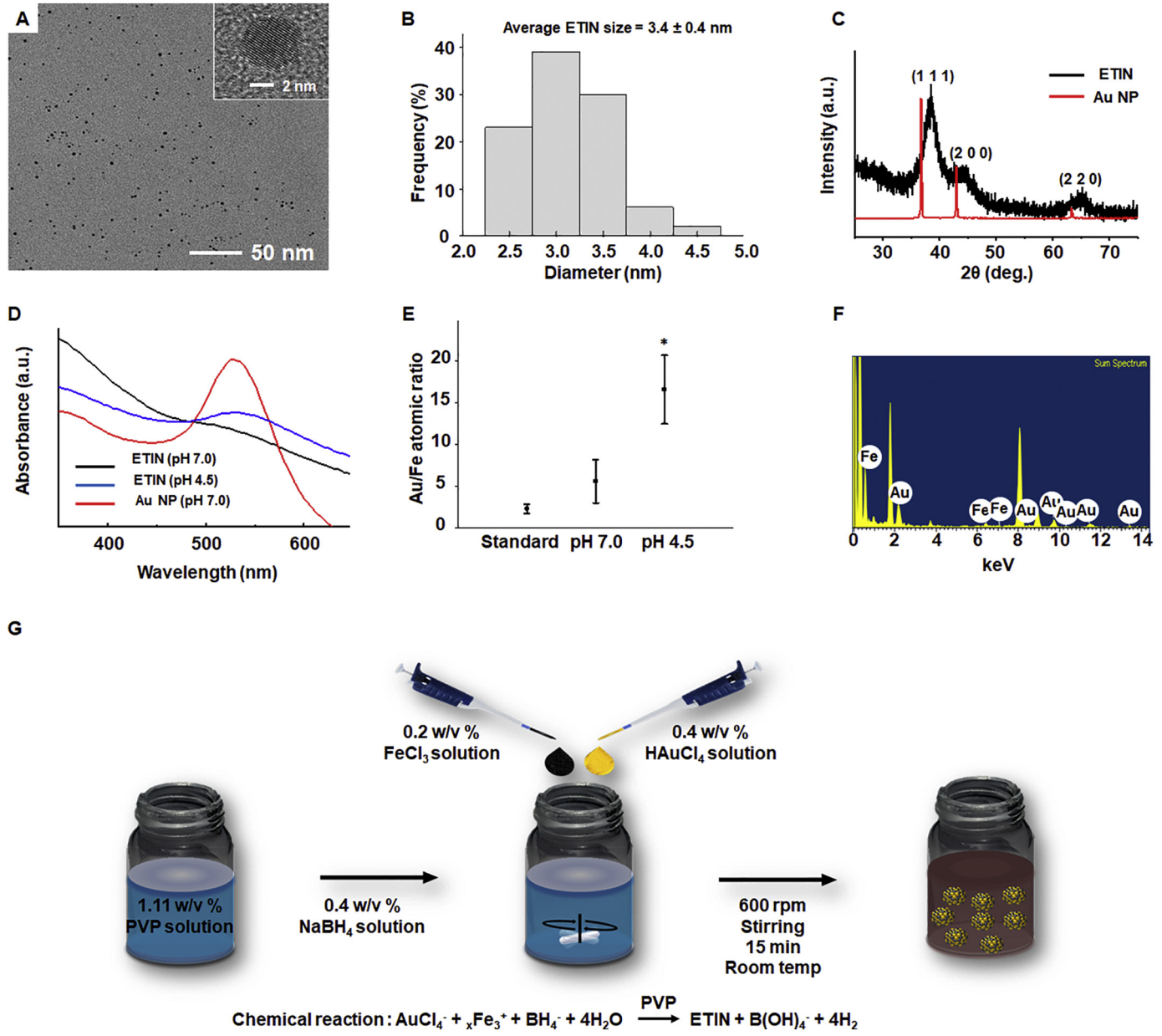

Fig. 1. Characterization of ETIN. (A) TEM images of pH-sensitive bioreducible ETIN (Inset: high-resolution TEM image of ETIN). (B) Size distribution of ETIN. (C) XRD patterns of NPs. (D) UV–Vis spectra of ETIN under acidic conditions (pH 4.5, 12 h, blue) and neutral conditions (pH 7.0, 12 h, black). Red lines indicate Au NPs exposed to neutral conditions (pH 7.0, 12 h). (E) Atomic ratio (Au/Fe) of ETIN according to the pH (pH 4.5 and 7.0, 12 h), as quantified by ICP-MS. ($n = 3$, $^*P < .05$ compared with other groups). (F) EDS profile of ETIN. (G) Schematic of the ETIN synthetic process. Abbreviation: TEM, transmission electron microscopy; XRD, X-ray powder diffraction; ICP-MS, inductively coupled plasma-mass spectroscopy; EDS, energy dispersive spectrometry. (For interpretation of the references to colour in this figure legend, the reader is referred to the web version of this article.)

in the no treatment (NT) group (Fig. 2E). However, when hMSCs were treated with ETIN concentration of 25 μg/mL or higher, cell viability decreased significantly while apoptotic activity increased significantly compared with the respective levels in the NT group. TUNEL staining revealed that a significant number of cells became apoptotic when hMSCs were exposed to 25 μg/mL or more of ETIN (Fig. 2F, white arrows). The effect of ETIN on cell morphology was observed through DiI staining (Fig. 2G). When the concentration of ETIN exceeded 25 μg/mL, a significant morphological change was induced in the hMSCs, and round and irregularly shaped cells were found, as indicated using white arrows in Fig. 2G [18]. The half maximal inhibitory concentration (IC50) value of ETIN was 41.58 μg/mL (Fig. S2). The optimized concentration of ETIN was considered to be less than 15 μg/mL.

2.3. ETIN upregulate the expression of angiogenic genes in hMSCs

We examined the expression of angiogenic growth factor genes *via* qRT-PCR. Fig. 3A shows that vascular endothelial growth factor (*VEGF*) mRNA expression was significantly increased in hMSCs treated with 5 and 15 μg/mL ETIN (1 h, serum-free medium), compared with that in the 0 μg/mL treatment group (NT, 1 h, serum-free medium). There was similar *VEGF* upregulation at 6 h and 12 h after treatment with 15 μg/mL of ETIN, compared with that at 1 h after treatment. However, *VEGF* gene expression was downregulated at 6 and 12 h in the NT and 5 μg/mL ETIN treatment groups. Fig. 3B shows that fibroblast growth factor 2 (*FGF2*) expression was also enhanced in the 5 and 15 μg/mL ETIN-treated hMSCs compared with that in the NT group (1 h, serum-free medium). In contrast to *VEGF* expression, *FGF2* expression was

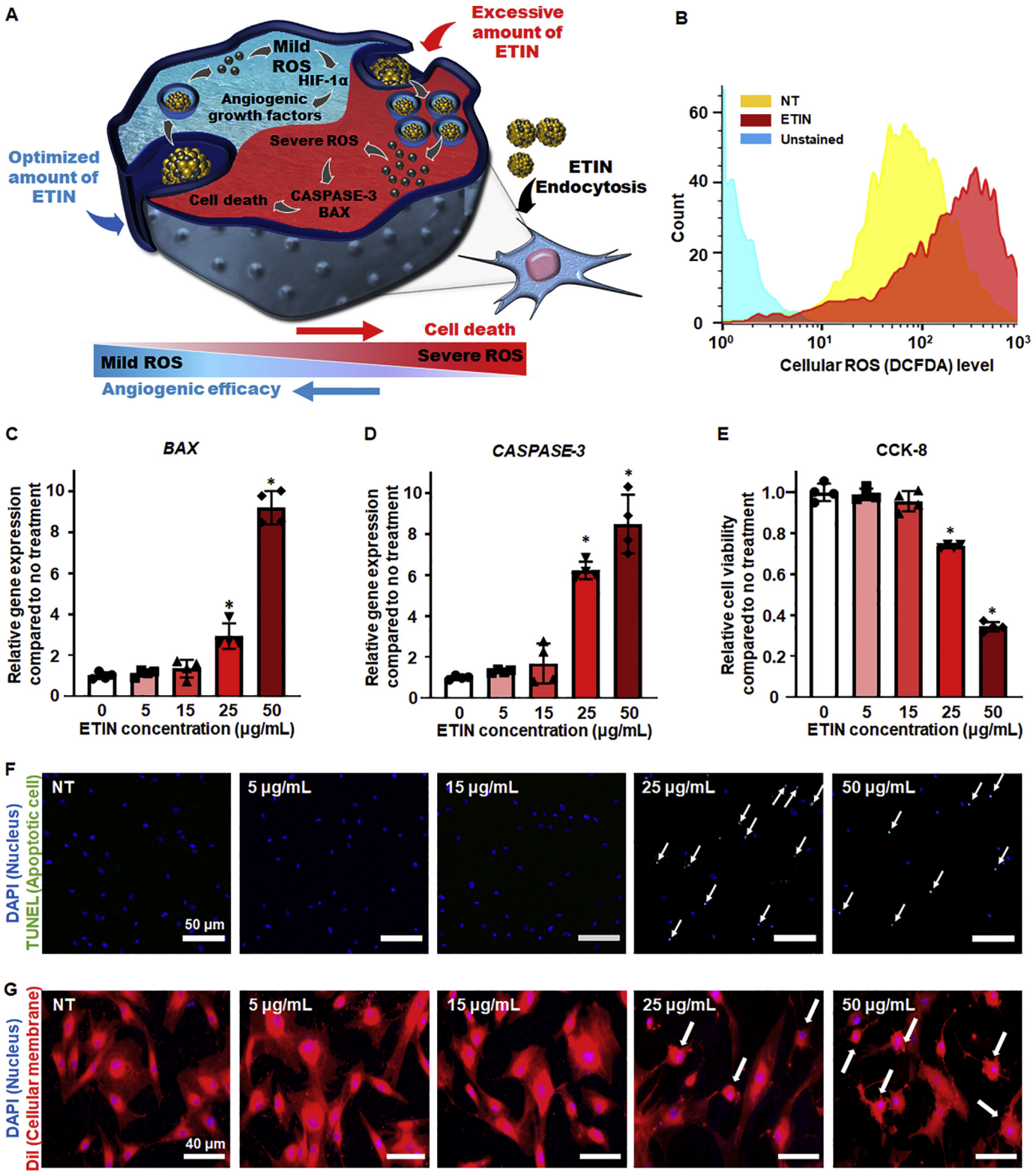

Fig. 2. Cytotoxicity of hMSCs treated with various concentrations of ETIN. (A) Schematic of intracellular, mild ROS generation induced by ETIN. (B) Intracellular ROS levels changed by ETIN treatment determined by FACS (DCFDA). Relative apoptotic mRNA expression of (C) *BAX* and (D) *CASPASE-3* in hMSCs treated with various concentrations of ETIN. (E) The viability of hMSCs after being treated with ETIN for 24 h ($n = 4$, $^*P < .001$ compared with no treatment group (NT)). (F) TUNEL staining (blue: nucleus; green: apoptotic cell) results from hMSCs treated with ETIN for 24 h. Scale bars indicate 50 μm. (G) DiI staining of hMSCs treated with ETIN for 24 h (blue: cell nucleus; red: cellular membrane). Scale bars indicate 40 μm. Abbreviation: FACS, fluorescence activated cell sorting; DCFDA, 2′,7′-dichlorodihydrofluorescein diacetate; TUNEL, terminal deoxynucleotide transferase-mediated deoxyuridine triphosphate nick end labeling; DiI, 1,1′-dioctadecyl-3,3,3′,3′-tetramethylindocarbocyanine perchlorate. (For interpretation of the references to colour in this figure legend, the reader is referred to the web version of this article.)

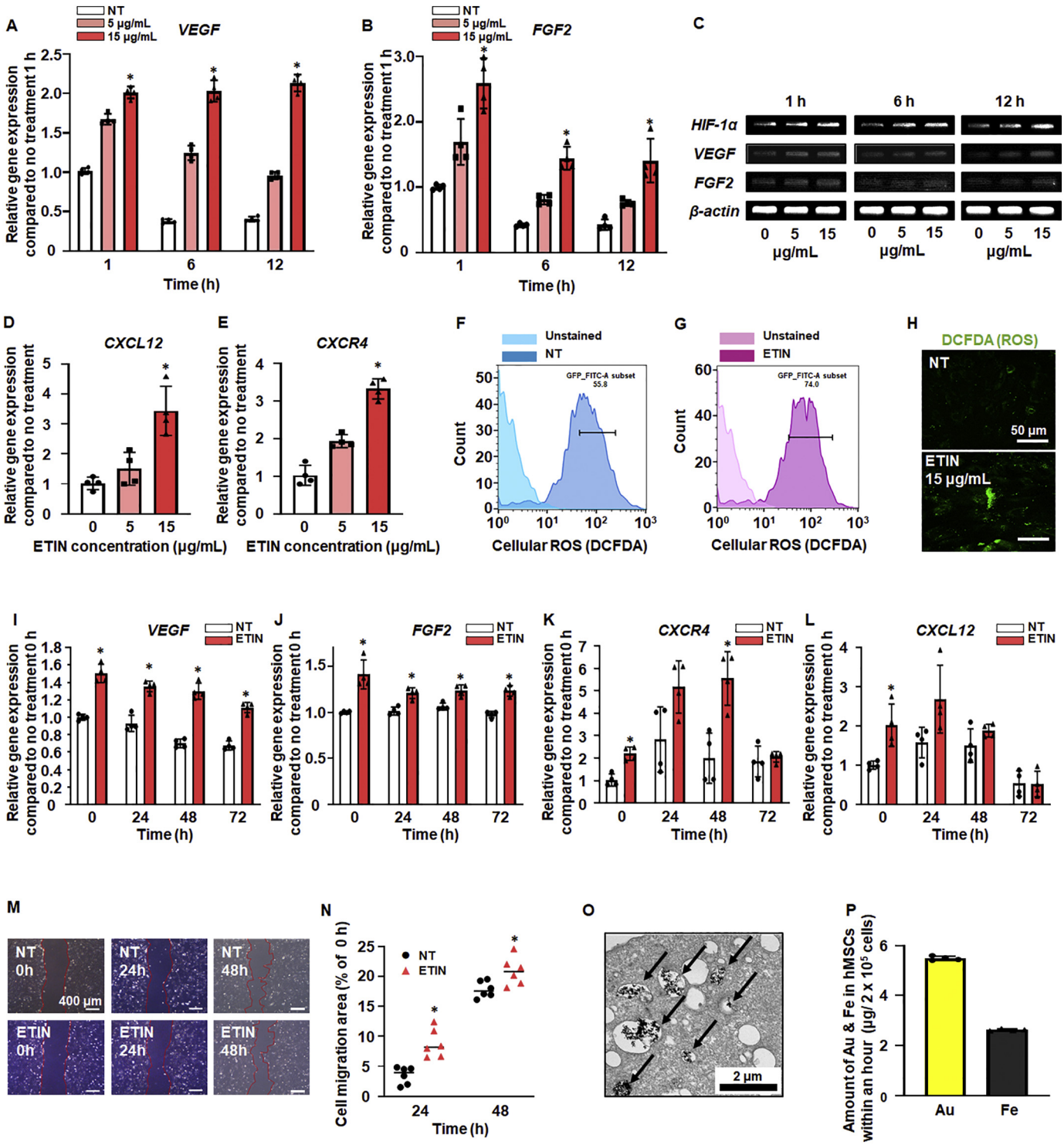

Fig. 3. Enhanced angiogenic growth factor production in hMSCs treated with ETIN. Relative mRNA expression of (A) *VEGF* and (B) *FGF2* in hMSCs treated with ETIN for various time periods ($n = 4$, $^*P < .05$ compared with all other groups). (C) Expression of angiogenesis-related genes in hMSCs after ETIN treatment. Relative mRNA expression of (D) *CXCL12* and (E) *CXCR4* in hMSCs after treatment with various concentrations of ETIN for 1 h (n = 4, $^*P < .05$ compared with all other groups). FACS results showing cellular ROS levels in (F) hMSCs without ETIN treatment and (G) hMSCs with 15 μg/mL of ETIN treatment ($n = 4$). (H) ROS assay results for hMSCs treated with (15 μg/mL) or without (0 μg/mL) ETIN (ROS; DCFDA, green). Scale bars indicate 50 μm. Duration of angiogenic growth factor and cell migration related gene expression in hMSCs after treatment with ETIN for 1 h. Duration of (I) *VEGF*, (J) *FGF2*, (K) *CXCR4*, and (L) *CXCL12* expression in hMSCs treated with ETIN for 1 h compared with that in the no treatment (NT) group (n = 4, $^*p < .05$ *versus* NT group). (M) Optical microscopy images illustrating cell migration of hMSCs treated with 15 μg/mL of ETIN (ETIN) and without ETIN (NT). (N) Average percentage of cell migration ($n = 6$, $^*P < .05$ *versus* NT group). (O) TEM images of hMSCs (black arrows indicate NPs in endosomes of hMSCs, scale bars indicate 2 μm). (P) Amount of cellular uptake of ETIN for 1 h, as determined by quantifying the amounts of Au and Fe in the hMSCs using ICP-MS (n = 4). (For interpretation of the references to colour in this figure legend, the reader is referred to the web version of this article.)

downregulated after 1 h in serum-free medium, regardless of ETIN concentration and time. Fig. 3C shows that the mRNA expression of the hypoxia-inducible factor-1 alpha (*HIF-1α)*, a key factor of the angiogenic signaling pathway in hMSCs, was increased in the 15 μg/mL ETIN-treated group. *VEGF* and *FGF2* expression were also enhanced when hMSCs were treated with 15 μg/mL of ETIN under serum-free culture conditions. The expression of C-X-C motif chemokine 12 (*CXCL12)* and *CXCR4* was the highest in hMSCs treated with 15 μg/mL of ETIN (1 h) compared with that in untreated hMSCs (Fig. 3D and E). ETIN induced a low increase in the levels of ROS (Fig. 3F–H), which is known to upregulate *HIF-1α* mRNA expression in hMSCs [10]. Therefore, considering the results from cytotoxicity and angiogenic gene expression profiling, 15 μg/mL of ETIN was chosen as the optimal concentration for the following *in vitro* and *in vivo* studies.

Prolonged exposure to ETIN for 72 h resulted in the persistently upregulated expression of *VEGF* and *FGF2* genes compared with the expression of these genes in the NT group (Fig. 3I and J). Similarly, *CXCR4* expression was also enhanced after treatment until 72 h, with a significant difference in mRNA levels between 0 and 48 h (Fig. 3K). The gene expression level of *CXCL12* was significantly changed immediately after treatment (0 h) (Fig. 3L). Based on the expression of *CXCR4* and *CXCL12* genes, a cell migration assay was performed to investigate whether the *in vitro* stem cell-homing capacity of ETIN-treated hMSCs can be increased. hMSCs showed a 2-fold increase in cell migration at 24 h and 48 h after treatment with ETIN, compared with the cell migration in the NT group (Fig. 3M and N); the upregulated expression of *CXCR4* and *CXCL12* may be the reason for the enhanced cellular migration ability of hMSCs. Expression of *HIF-1α* mRNA, the gene expression was upregulated for 12 h after ETIN treatment (Fig. S3). The cellular uptake of ETIN by hMSCs was also examined and TEM imaging of hMSCs confirmed the intracellular uptake of ETIN (Fig. 3O). The amount of NPs internalized by hMSCs after treatment was determined by quantifying the gold and iron in the cells using ICP-MS (Fig. 3P and Fig. S8). Based on ICP data shown in Fig. 3P, we calculated the encapsulation efficacy of ETIN (intracellular Fe concentration/total amount of Fe) to be 17.5 ± 0.3%. We added 15 μg/mL of Fe-ion solution to hMSCs for 3 h to confirm the effect of Fe-ion delivery to hMSCs *via* iron transporter and not endocytosis (Fig. S4). No significant differences were found in *VEGF* and *HIF-1α* gene expressions levels between hMSCs treated with the Fe-ion solution and those in the NT group.

2.4. ETIN prolong the enhanced gene expression in hMSCs

Treatment with 15 μg/mL of ETIN enhanced the cell viability of hMSCs compared with that of hMSCs without ETIN treatment under hypoxic culture conditions (2% O_2, serum-free medium) for 48 h (Fig. 4B and C); similar results were described for hMSCs cultured under hypoxic conditions with VEGF or FGF2 supplementation [19–22]. In addition, treatment of hMSCs with 15 μg/mL ETIN increased the antiapoptotic effect and enhanced *BCL-2* gene expression and decreased *CASPASE-3* gene expression when the hMSCs were exposed to hypoxic conditions for 48 h (Fig. 4D–G). The *BAX/BCL-2* expression ratio indicates the susceptibility of hMSCs to apoptosis [23]. The ETIN treatment group had a lower *BAX/BCL-2* ratio compared with that of the NT group (Fig. 4F), indicating an upregulated resistance to apoptosis in hMSCs with ETIN treatment. Hypoxic *in vitro* cell culture was applied to hMSCs with or without ETIN treatment to mimic the ischemic wound area with minimal blood flow in a wound-closing mouse model [24–27]. As shown in Fig. 4H and L, both hMSCs and human dermal fibroblasts (HDFs) supplemented with conditioned medium (CM) from hMSCs treated with ETIN (ETIN CM) proliferated significantly compared with cells supplemented with CM from hMSC without ETIN (hMSC CM). *KI67*, a cellular marker for proliferation, was significantly enhanced in both hMSCs and HDFs with ETIN CM supplementation compared with those with hMSC CM supplementation. In contrast, the expression of the *CASPASE-3* gene, a cellular marker for cell death, was downregulated upon ETIN CM supplementation in both hMSCs and HDFs compared with that upon hMSC CM supplementation (Fig. 4I, J, M, and N). Additionally, upregulated proliferation and downregulated cell death were also observed through FDA/EB staining in Fig. 4K and O. In addition, we have also investigated the expression of other angiogenesis-related proteins in the ETIN treated-hMSCs with ETIN CM supplementation (Fig. S7). Pro-angiogenic proteins such as pentraxin 3 [28], endoglin [29], endothelin-1 [30], FGF acidic [31], FGF basic [31], and urokinase plasminogen activator (uPA) [32] were more abundant in ETIN CM-supplemented cells than in NT CM; the anti-angiogenic protein, serpin F1 was downregulated in ETIN CM-supplemented cultures [33].

2.5. Enhanced cell viability in the ETIN-hMSC group after in vivo transplantation

After *in vivo* transplantation, the viability of hMSCs with ETIN treatment was significantly improved. Human nuclear antigen (HNA) staining showed more HNA^+ cells in the wounded area in the ETIN-hMSC group than in the other groups (Fig. 5B). Similar to HNA staining data, the amount of human *GAPDH* measured by RT-PCR was found to be the highest in the ETIN-hMSC group among all groups (Fig. 5C). As shown in Fig. 5D, human *VEGF* gene expression in the skin wound area was higher in the ETIN-hMSC group compared with that in the hMSC group. Transplantation of hMSCs has been known to downregulate the expression of pro-inflammatory cytokines, such as TNF-α and IL-12 [34]. The ETIN-hMSC group with enhanced hMSC viability had showed the lowest inflammation-related gene expression among all groups (Fig. 5E and F). Compared with the NT group, hMSCs with ETIN treatment enhanced the mouse Vimentin (fibroblast marker) gene expression (Fig. 5G) [35,36]. Interestingly, mouse VEGF gene expression from the entire wound region was significantly increased in the ETIN-hMSC group compared with that in the NT group (Fig. 5H).

2.6. Enhanced skin wound-healing by ETIN-hMSC transplantation

The wound-healing area at various times points is expressed as a percentage relative to the original wound size. Seven days after transplantation with or without cells, the wound areas were not significantly different among the groups (Fig. 6A). However, the ETIN-treated groups showed a significantly enhanced wound-healing ratio (96.2 ± 3.0%) compared with those of the other groups 14 days after treatment (Fig. 6C). The wound size of the hMSC group was not significantly different from that of the NT group at day 14 (80.3 ± 5.8 and 72.0 ± 7.5%, respectively). The best wound-healing results based on the histological structure after H&E and Masson's trichrome staining for the ETIN-hMSC group compared with those for the other groups at day 14 are shown in Fig. 6D and E. In the ETIN-hMSC group, muscle cells migrated to the wounded area from the side and collagen deposition was improved compared with that in the other groups. However, the NT and hMSC groups showed incomplete epithelialization in the wounded area, compared with the ETIN-hMSC group. To investigate the degree of angiogenesis, blood vessels in the skin wound were immunostained with anti-CD31 and anti-SM-α antibodies and mRNA expression was evaluated by qRT-PCR (Fig. 6F–H). Fig. 6F shows that the number of $CD31^+$ blood vessels was highest in the ETIN-hMSC group. Similarly, there were 3.1-fold and 1.8-fold increases in CD31 gene expression in the ETIN-hMSC group compared with that in the NT group and hMSC group, respectively (Fig. 6G). However, the number of SM-α^+ vessels and SM-α gene expression were not significantly different among the groups. Fig. 6I and J indicate that the ETIN-hMSC group showed significantly enhanced regeneration in the epidermis layer and basal layer, compared with the other groups.

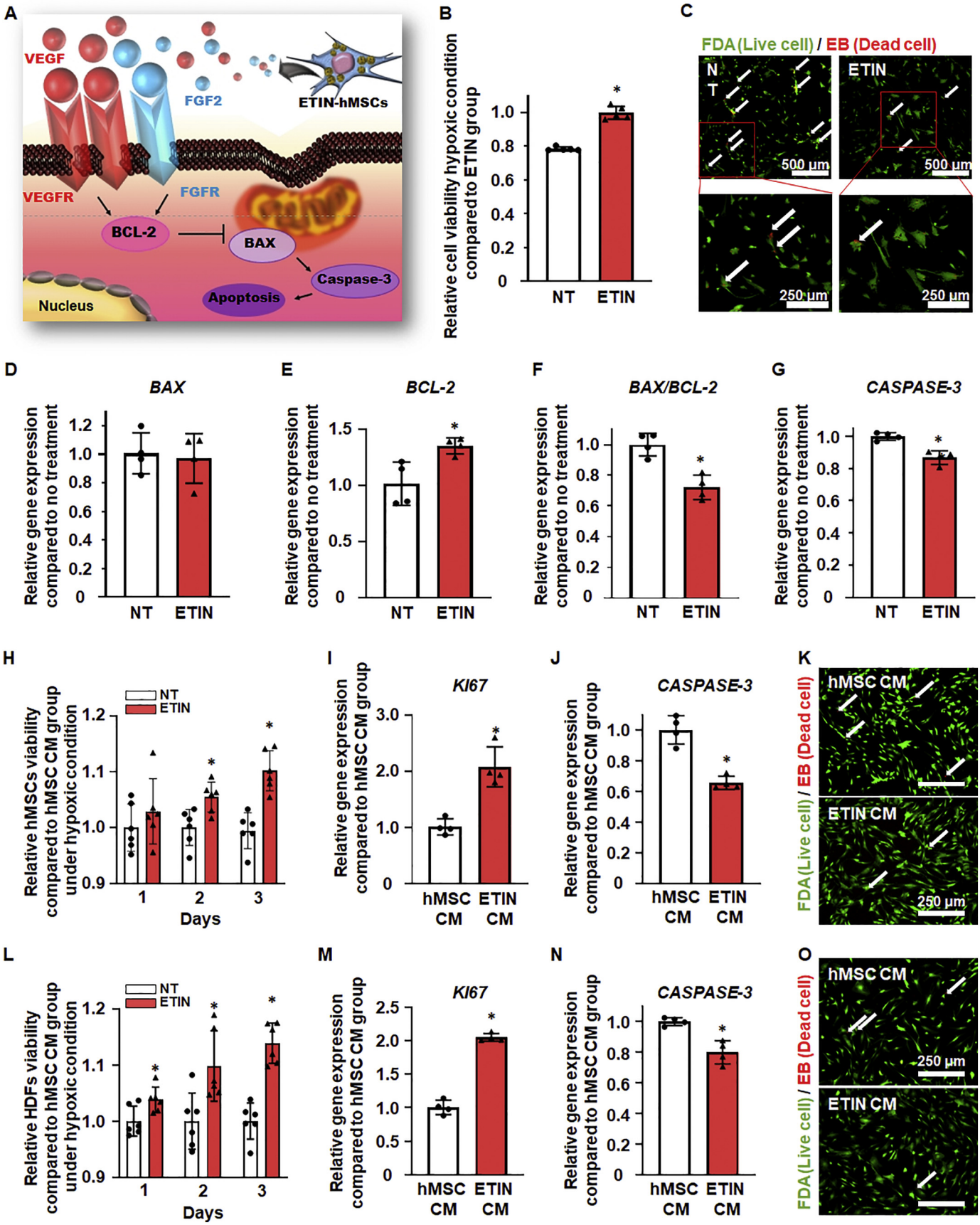

(caption on next page)

Fig. 4. Cell viability of hMSCs with ETIN treatment (15 μg/mL) induced by upregulated *VEGF* and *FGF2* secretion under hypoxic conditions (2% O_2 and serum-free medium for 48 h). (A) Schematic of the antiapoptotic mechanism. (B) The viability of hMSCs under hypoxic conditions without or with ETIN treatment ($n = 8$, $^*P < .001$ *versus* ETIN group). (C) Fluorescein diacetate and ethidium bromide (FDA/EB) assay to observe cell viability with or without ETIN treatment under hypoxic conditions. Green colour indicates live cells and red colour indicates dead cells (white arrows). Red boxed regions are magnified (bottom). Relative mRNA expression of (D) *BAX*, (E) *BCL-2*, (F) *BAX/BCL-2* ratio, and (G) *CASPASE-3* in hMSCs treated without or with ETIN under hypoxic conditions, as determined by qRT-PCR ($n = 4$, $^*P < .05$ *versus* NT group). (H) Relative viability of hMSCs supplemented with conditioned medium extracted from hMSCs with ETIN treatment (ETIN CM) compared with that of hMSCs supplemented with conditioned medium extracted from hMSCs without ETIN treatment (hMSC CM) under hypoxic conditions ($n = 6$, $^*P < .05$ *versus* hMSC CM group). Relative mRNA expression of (I) *KI67* and (J) *CASPASE-3* from hMSCs treated with ETIN CM compared with that of hMSCs treated with hMSC CM under hypoxic conditions for 3 days (n = 4, $^*P < .05$ *versus* hMSC CM group). (K) FDA/EB assay to measure the viability of hMSCs treated with hMSC CM or ETIN CM under hypoxic conditions for 3 days. Green colour indicates live cells and red colour indicates dead cells (white arrows). (L) Relative viability of human dermal fibroblasts (HDFs) supplemented with ETIN CM compared with that of HDFs supplemetned with hMSC CM under hypoxic conditions (n = 6, $^*P < .05$ *versus* hMSC CM group). Relative mRNA expression of (M) *KI67* and (N) *CASPASE-3* from HDFs treated with hMSC CM or ETIN CM under hypoxic conditions for 3 days (n = 4, $^*P < .05$ *versus* hMSC CM group). (O) FDA/EB assay for the viability of HDFs supplemented with hMSC CM or ETIN CM under hypoxic conditions for 3 days. Live cells are stained green and dead cells (white arrows) are stained red. Abbreviation: FDA/EB, fluorescein diacetate/ethidium bromide. (For interpretation of the references to colour in this figure legend, the reader is referred to the web version of this article.)

3. Discussion

MSC therapy has been known as a potential method for tissue regeneration. However, because of the harsh microenvironment in the wound area, transplanted MSCs exhibit a low survival rate and poor sequential angiogenesis and tissue repair. Therefore, enhancing the survival rate and cytokine expression of MSCs for angiogenesis can be a solution to overcome this limitation. In this study, hMSCs were treated with ETIN, which enhanced hMSCs viability even under hypoxic cell culture conditions and improved the expression of angiogenic paracrine factors. *In vivo* tests additionally demonstrated that hMSCs treated with ETIN downregulated the gene expression of initial inflammation markers and upregulated the migration of fibroblasts to the wound site. To the best of our knowledge, this is the first study to report the therapeutic effects of ETIN applied to hMSCs as a therapeutic material related with early stage inflammation, migration of host derived cells, and enhancement of therapeutic angiogenesis. Fig. 2A shows that pH-sensitive ETIN delivered Fe ions in an intracellular manner without causing severe cytotoxicity. We controlled the amount of Fe ions released to induce mild intracellular ROS in hMSCs by quantitative control of ETIN (Fig. 3F–H). Upregulated HIF-1α expression induced by mild intracellular ROS generation enhanced the secretion of angiogenic factors from and the migration capacity of hMSCs by upregulating *VEGF* [37], *FGF2* [38], *CXCR4* [39,40], and *CXCL12* [39,40] mRNA expression. Therefore, through the upregulation of specific genes, we conclude that hMSCs can undergo hypoxic preconditioning and, thus, have an enhanced cell viability after transplantation to ischemic regions [41,42].

In this study, ETIN were applied to hMSCs as a therapeutic material. To the best of our knowledge, few studies have analyzed gold-iron nanoparticles [43,44]. Previous studies manipulated NPs in an organic solvent such as octyl ether, or used high temperature with a toxic organic solvent to fabricate similar nanoparticles, which makes it difficult for NPs to be applied in biomedical research. In addition, conventional Fe-based nanoparticles, which represent inorganic nanoparticles (INPs), are normally used as a bioimaging tool [45] and not as a therapeutic material; for example, Fe_3O_4/carbon nanoparticles were recently reported to be used in magnetic resonance imaging [46]. Herein, we synthesized ecologically-friendly and low-toxicity ETIN for use as a therapeutic substance and observed the improvement in the wound-healing effect of ETIN-laden hMSCs. For making ETIN, we used an environmentally friendly method using a low temperature and water-based approach at atmospheric pressure (Fig. 1H).

A previous report has shown that a higher cell density can induce a decrease in CXCR4 expression [47]. Therefore, despite the enhanced CXCR4 expression in the ETIN-hMSC group, the higher cell density at 48 and 72 h may have down-regulated CXCR4 expression compared with that at earlier time points. Another report has shown that the accumulation of FGF2 can inhibit the CXCL12 expression through FGFR1 IIIc expression [48]. An increase in *HIF-1α* gene expression in hMSCs after ETIN treatment was apparent until 12 h compared with that in the hMSC (Fig. S3) and then decreased by 24 h after ETIN treatment; however, there was no significant difference in *HIF-1α* gene expression between hMSCs with or without ETIN treatment.

Continuously upregulated VEGF and FGF2 expression up to 72 h after ETIN treatment may enhance blood vessel development in the wound area [24,49]. Furthermore, *VEGF* and *FGF2* were reported to show antiapoptotic effects and, thus enhance cell survival [24,25]. We cultured hMSCs under hypoxic conditions to mimic the physiological conditions of the wounded area where blood vessels are rare before *in vivo* tests [26,27]. As shown in Fig. 4, The expression of the anti-apoptotic gene, *BCL-2*, was enhanced by upregulated *VEGF* and *FGF2* gene expression [19,50]. *BCL-2* gene expression inhibits the expression of the pro-apoptotic gene, *BAX*, which sequentially upregulates *CASPASE-3* expression and eventually induces apoptosis in hMSCs [51]. Treatment of hMSCs with ETIN upregulated HIF-1α expression and enabled hMSC hypoxic preconditioning, which may be beneficial for cell therapy [52,53]. hMSCs and HDFs play critical roles in the inflammatory and re-epithelialization phases of wound-healing [54,55] and showed significantly enhanced proliferation and cell viability after supplementation with ETIN CM (Fig. 4H–O). Based on Figs. 3 and 5 and S8, we concluded that enhanced VEGF, FGF2, pentraxin 3 [28], endoglin [29], endothelin-1 [30], FGF acidic [31], FGF basic [31], and uPA [32] secreted from ETIN-hMSCs could have improved the wound-healing process compared with conventional treatment; additionally, the anti-angiogenic protein, serpin F1 was downregulated [33]. Similar to the *in vitro* test, as shown in Fig. 4A–G, the enhanced hMSC survival rate in the ETIN-hMSC group could have increased the therapeutic effect of ETIN (Figs. 5 and 6). In Fig. 5E and F, pro-inflammatory cytokines such as TNF-α and IL-12 were significantly decreased in the ETIN-MSC group compared with those in the other groups, thus reducing severe inflammation and enhancing wound-healing efficacy [34]. Fibroblasts also play vital roles during the wound-healing process [56,57]. In our research, enhanced HDF proliferation and upregulated Vimentin gene expression were observed (Figs. 4L–O and 5). Vimentin expression may be particularly important as it promotes the proliferation of fibroblasts and collagen accumulation [35,36]. Therefore, the wound-healing process may have been accelerated *via* decreased inflammation and increased fibroblast activity (Fig. 5).

We also investigated how *in vivo* angiogenesis and wound closure were affected by upregulated angiogenic growth factors in the ETIN-treated group. We demonstrated that the ETIN-hMSC group significantly increased the number of $CD31^+$ microvessels in the skin wound region (Fig. 6H). The enhancement in the *in vivo* angiogenesis in the ETIN-hMSC group may have been caused by the improvement of cell viability and increase in angiogenic paracrine factor expression, compared with those in the other groups. In addition, upregulated *CXCR4* and *CXCL12* expression may enhance cell migration to the wound sites, increasing the wound-healing rate [10,58,59]. *CXCR4* and *CXCL12* expression improved the localization of hMSCs to the wound

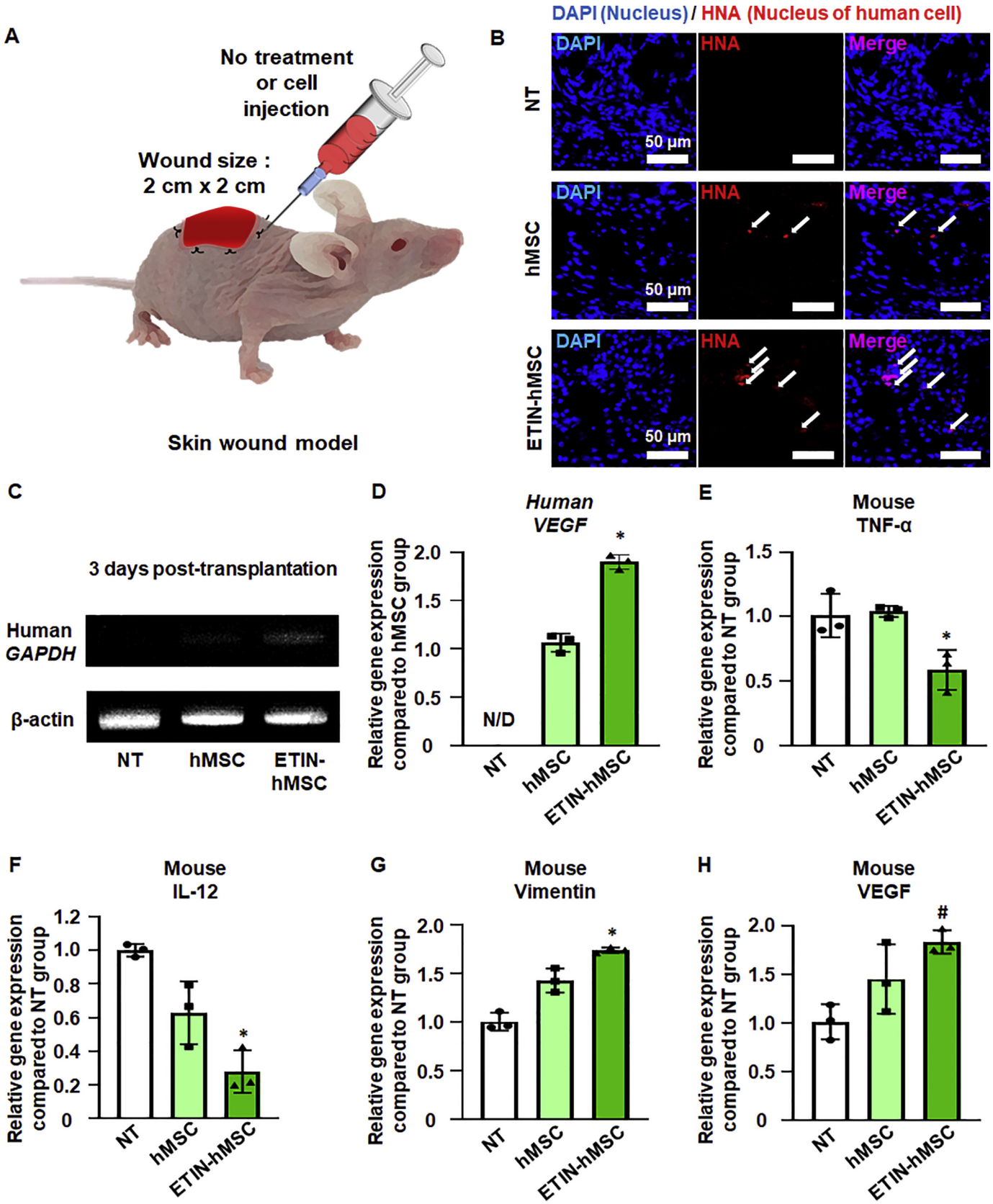

Fig. 5. Enhanced expression of hMSC viability and wound-healing related genes in the ETIN-treated group three days after transplantation. (A) Schematic diagram of the mouse skin wound model. (B) Co-staining with DAPI (blue: nucleus) and human nuclear antigen (HNA, red: human cell) at the skin wound site. (C) Expression of human *GAPDH* and mouse and human *β-actin* to compare the numbers of hMSCs remaining in the wounded area. Relative gene expression for (D) human *VEGF*, (E) mouse TNF-α, and (F) mouse IL-12, (G) mouse Vimentin, (H) mouse VEGF from wound regions at 3 days after treatment (N/D: not detected (Fig. 5D), $n = 3$, $^{*}P < .05$ compared to all other groups, $^{\#}P < .05$ compared to no treatment (NT) group). Abbreviation: HNA, human nucleus antigen; IL-12, interleukin-12. (For interpretation of the references to colour in this figure legend, the reader is referred to the web version of this article.)

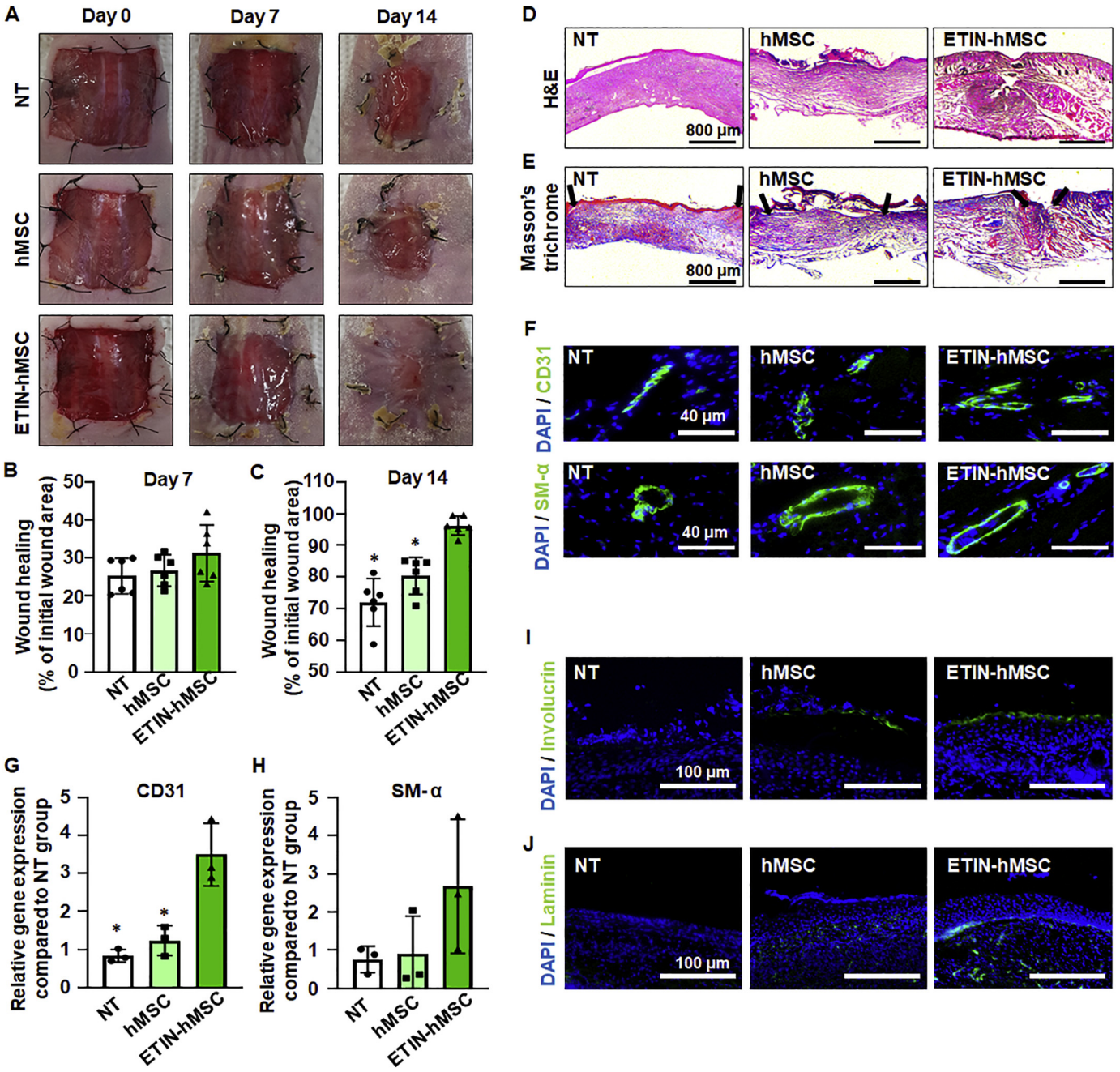

Fig. 6. Improved wound closing induced by ETIN-treated hMSCs in mouse skin wound model. (A) Representative photographs of full-thickness skin wounds on day 0, 7, and 14 after attaching Tegaderm over the wound site without treatment (NT group), with hMSC injection (hMSC group, 10^6 cells/200 μL of phosphate buffered saline [PBS]), and treatment with ETIN-laden hMSCs (ETIN-hMSC group, 15 μg/mL, 10^6 cells/200 μL of PBS). Wound closure rates on day 7 (B) and 14 (C). (*$P < .001$ *versus* ETIN-hMSC group, as analyzed by two-way repeated measures ANOVA followed by Bonferroni *t*-test). (D) Representative images of hematoxylin and eosin (H&E)-stained sections (wound-healing regions on day 14 after treatments). Scale bars indicate 800 μm. (E) Representative images of Masson's trichrome-stained sections (wound-healing regions on days 14 after wounding and treatments). Black arrows indicate initial wound area. Scale bars indicate 800 μm. (F) Immunostaining of CD31 (green) or smooth muscle alpha actin (SM-α, green) in wound-healing regions on day 14 after wounding and treatments. Blue indicates DAPI. Scale bars indicate 40 μm. (G, H) Analysis of gene expression by qRT-PCR of representative vascular marker (CD31 and SM-α) from wound sites on day 14 after wounding and treatments ($n = 4$, *$P < .05$ *versus* ETIN-hMSC group). Representative images of immunostaining of (I) involucrin and (J) at the wound bed on day 14 after wounding and treatments. Blue indicates DAPI. Scale bars indicate 100 μm. Abbreviation: SM-α, smooth muscle alpha actin. (For interpretation of the references to colour in this figure legend, the reader is referred to the web version of this article.)

sites for tissue restoration and neovascularization [60–64]. Furthermore, upregulated wound-healing was accompanied by an improvement in re-epithelization in the ETIN-hMSC groups with enhanced involucrin and laminin expression (Fig. 6I and J). Involucrin is a protein expressed in keratinocytes in the epidermis, and laminin is a component of the basal lamina layer. Based on upregulated involucrin and laminin expression, we conclude that ETIN-hMSCs could significantly enhance the regeneration of the epidermis and the basal layer in wound areas compared with conventional hMSC transplantation.

4. Conclusion

In this work, we demonstrate for the first time that INPs can be applied to hMSCs as a therapeutic material related with early stage

inflammation, the migration of host-derived cells, and the enhancement of therapeutic angiogenesis by intracellular ROS control. Additionally, the Au in ETIN that was used as an indicator of INP delivery can be applied for non-invasive bioimaging [65], which can be adopted in further studies. The ecologically-friendly synthesis of ETIN and the upregulated therapeutic efficacy induced by the intracellular ROS control in stem cells may lead to a wide range of new applications in tissue regeneration using INPs.

5. Materials and methods

5.1. Synthesis of ETIN

ETIN was synthesized based on co-reduction method. Poly(vinyl pyrrolidone) (PVP, Sigma-Aldrich, St. Louis, MO, USA) was fully dissolved in DI-water at RT. Sodium borohydride ($NaBH_4$, Sigma-Aldrich) solution was infused in PVP solution. With constant stirring of PVP added $NaBH_4$ solution, dropwise (slowly) Gold (III) chloride hydrate ($HAuCl_4{\cdot}xH_2O$, Sigma) solution and iron (III) chloride ($FeCl_3$, Sigma) solution were injected into the solution.

5.2. Fe-ion release from the ETIN under acidic conditions

The amount of Fe ions released from the ETIN at different pH conditions was determined using UV–Vis spectroscopy (Cary 60 UV–vis, Agilent Technologies, Santa Clara, USA) and EDS (JEM-2100F, JEOL). A pH of 4.5 was considered as the microenvironment of the endosome, and pH 7 was considered as a neutral condition of the cell culture medium. HCl was added to PBS (Gibco BRL, Gaithersburg, MD, USA) solution to adjust the pH to the two different values (4.5 and 7.0). The ETIN were then dispersed in PBS with different pH values of 4.5 and 7.0 at RT. After 12 h, each sample was centrifuged to separate the NPs from PBS. The NPs were analyzed with EDS to confirm the Au/Fe ratio.

5.3. Reactive oxygen species (ROS) assay

ROS was measured using the fluorescent indicator DCFDA (D339 Invitrogen, Carlsbad, USA). After ETIN treatment, the cells were incubated with 10 μM DCFDA in PBS solution for 20 min at 37 °C. After staining, the samples were washed twice with PBS or FACS buffer solution and examined by fluorescence microscopy (IX71, Olympus) and FACS using a flow cytometer (MACSQuant® VYB, Miltenyi Biotec, Bergisch-Gladbach, Germany).

5.4. Migration assay

hMSCs were grown to confluence in 6-well plates. Next, the cells were incubated with or without ETIN for 1 h. A straight scratch was made on the hMSCs using a P200 pipette tip. The cells were then washed with PBS three times, and further cultured in DMEM. After incubation for 0, 24, and 48 h, the width of the re-populating scratch gap was measured and recorded and then compared with the initial gap size at 0 h [66]. The Photoshop CC program (Adobe Systems, San Jose, CA, USA) was used to determine the size of the gap at each time point from digital images [67].

5.5. Analysis of the ETIN CM components

To identify proteins from the CM, 1 mL of the basal medium, 1 mL of the NT CM and ETIN CM were each loaded onto cytokine and angiogenesis array membrane (R&D systems, Inc., Minneapolis, Minnesota, USA). After blocking the array membrane with blocking buffer for 1 h and membrane washing, the each of CM and array detection antibody cocktail was mixed and added to the blocked membrane followed by overnight shaking incubation at 4 °C. After washing, streptavidin-HRP buffer was added to the membrane, and incubation was performed for 30 min. Following another washing, Chemi Reagent Mixture was added to the membrane for reaction at room temperature and measured using LAS-3000 system (Fujifilm, Tokyo, Japan).

Acknowledgments

Kazunori Kataoka at the University of Tokyo and Kawasaki Institute of Industrial Promotion in Japan is acknowledged for his helpful advices on the manuscript development. This research was supported by the National Research Foundation of Korea (NRF), funded by the Ministry of Science and ICT (NRF-2018M3A9E2023255, NRF-2017R1A5A1070259, NRF-2017R1A5A1015365, and NRF-2019R1C1C1007384); by the Bio & Medical Technology Development Program of the NRF funded by the Ministry of Science, ICT and Future Planning (NRF-2016M3A9B4919711) and by a grant of the Korea Health Technology R&D Project through the Korea Health Industry Development Institute (KHIDI), funded by the Ministry of Health & Welfare, Republic of Korea (grant HI17C1728). This work was supported by the NRF grant funded by the Korean government (MSIP) (NRF-2014R1A5A1009799, NRF- 2019M3E6A1103866, and NRF-2016M3D1A1021140).

Appendix A. Supplementary data

Supplementary data to this article can be found online at https://doi.org/10.1016/j.jconrel.2020.05.038.

References

[1] S.Y. Kwak, T.T.S. Lew, C.J. Sweeney, V.B. Koman, M.H. Wong, K. Bohmert-Tatarev, K.D. Snell, J.S. Seo, N.H. Chua, M.S. Strano, Chloroplast-selective gene delivery and expression in planta using chitosan-complexed single-walled carbon nanotube carriers, Nat. Nanotechnol. 14 (2019) 447–455.
[2] P.D. Ramírez-García, J.S. Retamal, P. Shenoy, W. Imlach, M. Sykes, N. Truong, L. Constandil, T. Pelissier, C.J. Nowell, S.Y. Khor, L.M. Layani, C. Lumb, D.P. Poole, T. Lieu, G.D. Stewart, Q.N. Mai, D.D. Jensen, R. Latorre, N.N. Scheff, B.L. Schmidt, J.F. Quinn, M.R. Whittaker, N.A. Veldhuis, T.P. Davis, N.W. Bunnett, A pH-responsive nanoparticle targets the neurokinin 1 receptor in endosomes to prevent chronic pain, Nat. Nanotechnol. 14 (2019) 1150–1159.
[3] K.C. Kwon, E. Jo, Y.W. Kwon, B. Lee, J.H. Ryu, E.J. Lee, K. Kim, J. Lee, Superparamagnetic gold nanoparticles synthesized on protein particle scaffolds for cancer theragnosis, Adv. Mater. 29 (2017) 1701146.
[4] Y. Sun, Y. Xia, Shape-controlled synthesis of gold and silver nanoparticles, Science 298 (2002) 2176–2179.
[5] A. Albanese, P.S. Tang, W.C. Chan, The effect of nanoparticle size, shape, and surface chemistry on biological systems, Annu. Rev. Biomed. Eng. 14 (2012) 1–16.
[6] K. Kamei, Y. Mukai, H. Kojima, T. Yoshikawa, M. Yoshikawa, G. Kiyohara, T.A. Yamamoto, Y. Yoshioka, N. Okada, S. Seino, S. Nakagawa, Direct cell entry of gold/iron-oxide magnetic nanoparticles in adenovirus mediated gene delivery, Biomaterials 30 (2009) 1809–1814.
[7] S.D. Perrault, C. Walkey, T. Jennings, H.C. Fischer, W.C. Chan, Mediating tumor targeting efficiency of nanoparticles through design, Nano Lett. 9 (2009) 1909–1915.
[8] E.A. Sykes, Q. Dai, K.M. Tsoi, D.M. Hwang, W.C. Chan, Nanoparticle exposure in animals can be visualized in the skin and analysed via skin biopsy, Nat. Commun. 5 (2014) 3796.
[9] B.H. Mao, Z.Y. Chen, Y.J. Wang, S.J. Yan, Silver nanoparticles have lethal and sublethal adverse effects on development and longevity by inducing ROS-mediated stress responses, Sci. Rep. 8 (2018) 2445.
[10] S. Avniel, Z. Arik, A. Maly, A. Sagie, H.B. Basst, M.D. Yahana, I.D. Weiss, B. Pal, O. Wald, D. Ad-El, N. Fujii, F. Arenzana-Seisdedos, S. Jung, E. Galun, E. Gur, A. Peled, Involvement of the CXCL12/CXCR4 pathway in the recovery of skin following burns, J. Invest. Dermatol. 126 (2006) 468–476.
[11] X. Huang, F. Zhang, Y. Wang, X. Sun, K.Y. Choi, D. Liu, J. Choi, T.-H. Shin, T.J. Cheon, G. Niu, X. Chen, Correction to design considerations of iron-based nanoclusters for noninvasive tracking of mesenchymal stem cell homing, ACS Nano 8 (2014) 4403–4414.
[12] S.J. Dixon, B.R. Stockwell, The role of iron and reactive oxygen species in cell death, Nat. Chem. Biol. 10 (2014) 9–17.
[13] W.M. Haynes, CRC Handbook of Chemistry and Physics, CRC Press, 2012, p. 8e25.
[14] B. Zhao, X. Li, Y. Wang, P.J. Shang, Iron-dependent cell death as executioner of cancer stem cells, Exp. Clin. Cancer Res. 37 (2018) 79.
[15] F. Mazuel, A. Espinosa, N. Luciani, M. Reffay, R. Le Borgne, L. Motte, K. Desboeufs, A. Michel, T. Pellegrino, Y. Lalatonne, C. Wilhelm, Massive intracellular biodegradation of iron oxide nanoparticles evidenced magnetically at single-endosome and tissue levels, ACS Nano 10 (2016) 7627–7638.
[16] C. Li, K.L. Shuford, M. Chen, E.J. Lee, S.O. Cho, A facile polyol route to uniform gold

octahedra with tailorable size and their optical properties, ACS Nano 2 (2008) 1760–1769.
[17] M. Redza-Dutordoir, D.A. Averill-Bates, Activation of apoptosis signalling pathways by reactive oxygen species, Biochim. Biophys. Acta 1863 (2016) 2977–2992.
[18] S. Povea-Cabello, M. Oropesa-Ávila, P. de la Cruz-Ojeda, M. Villanueva-Paz, M. de la Mata, J. Suárez-Rivero, M. Álvarez-Córdoba, I. Villalón-García, D. Cotán, P. Ybot-González, J. Sánchez-Alcázar, Dynamic reorganization of the cytoskeleton during apoptosis: the two coffins hypothesis, J. Int. J. Mol. Sci. 18 (2017) 2393.
[19] H. Song, K. Kwon, S. Lim, S.M. Kang, Y.G. Ko, Z. Xu, J.H. Chung, B.S. Kim, H. Lee, B. Joung, S. Park, D. Choi, Y. Jang, N.S. Chung, K.J. Yoo, K.C. Hwang, Transfection of mesenchymal stem cells with the FGF-2 gene improves their survival under hypoxic conditions, Mol. Cells 19 (2005) 402–407.
[20] S.H. Bhang, T.-J. Lee, W.-G. La, D.-I. Kim, B.-S. Kim, Delivery of fibroblast growth factor 2 enhances the viability of cord blood-derived mesenchymal stem cells transplanted to ischemic limbs, J. Biosci. Bioeng. 111 (2011) 584–589.
[21] H.-H. Moon, M.K. Joo, H. Mok, M. Lee, K.-C. Hwang, S.W. Kim, J.H. Jeong, D. Choi, S.H. Kim, MSC-based VEGF gene therapy in rat myocardial infarction model using facial amphipathic bile acid-conjugated polyethyleneimine, Biomaterials 35 (2014) 1744–1754.
[22] Y. Tang, X. Gan, R. Cheheltani, E. Curran, G. Lamberti, B. Krynska, M.F. Kiani, B. Wang, Targeted delivery of vascular endothelial growth factor improves stem cell therapy in a rat myocardial infarction model, Nanomedicine 10 (2014) 1711–1718.
[23] F. Yin, L. Guo, C. Meng, Y. Liu, R. Lu, P. Li, Y. Zhou, Transplantation of mesenchymal stem cells exerts anti-apoptotic effects in adult rats after spinal cord ischemia-reperfusion injury, Brain Res. 1561 (2014) 1–10.
[24] K. Gupta, S. Kshirsagar, W. Li, L. Gui, S. Ramakrishnan, P. Gupta, P.Y. Law, R.P. Hebbel, VEGF prevents apoptosis of human microvascular endothelial cells via opposing effects on MAPK/ERK and SAPK/JNK signaling, Exp. Cell Res. 247 (1999) 495–504.
[25] I. Ay, H. Sugimori, S.P. Finklestein, Intravenous basic fibroblast growth factor (bFGF) decreases DNA fragmentation and prevents downregulation of Bcl-2 expression in the ischemic brain following middle cerebral artery occlusion in rats, Mol. Brain Res. 87 (2001) 71–80.
[26] K. Jia, D. Sun, S. Ling, Y. Tian, X. Yang, J. Sui, B. Tang, L. Wang, Activated δ-opioid receptors inhibit hydrogen peroxide-induced apoptosis in liver cancer cells through the PKC/ERK signaling pathway, Mol. Med. Rep. 10 (2014) 839–847.
[27] U. Nekanti, S. Dastidar, P. Venugopal, S. Totey, M. Ta, Increased proliferation and analysis of differential gene expression in human Wharton's jelly-derived mesenchymal stromal cells under hypoxia, Int. J. Biol. Sci. 6 (2010) 499–512.
[28] I. Rajkovic, R. Wong, E. Lemarchand, J. Rivers-Auty, O. Rajkovic, C. Garlanda, S.M. Allan, E. Pinteaux, Pentraxin 3 promotes long-term cerebral blood flow recovery, angiogenesis, and neuronal survival after stroke, J. Mol. Med. 96 (2018) 1319–1322.
[29] L. Jonker, H.M. Arthur, Endoglin expression in early development is associated with vasculogenesis and angiogenesis, Mech. Dev. 110 (2002) 193–196.
[30] D. Salani, G. Taraboletti, L. Rosanò, V. Di Castro, P. Borsotti, R. Giavazzi, A. Bagnato, Endothelin-1 induces an angiogenic phenotype in cultured endothelial cells and stimulates neovascularization in vivo, Am. J. Pathol. 157 (2000) 1703–1711.
[31] T. Zhao, W. Zhao, Y. Chen, R.A. Ahokas, Y. Sun, Acidic and basic fibroblast growth factors involved in cardiac angiogenesis following infarction, Int. J. Cardiol. 152 (2011) 307–313.
[32] C.W. Oh, J. Hoover-Plow, E.F. Plow, The role of plasminogen in angiogenesis in vivo, J. Thromb. Haemost. 1 (2008) 1683–1687.
[33] J.G. Ren, C. Jie, C. Talbot, How PEDF prevents angiogenesis: a hypothesized pathway, Med. Hypotheses 64 (2005) 74–78.
[34] D.E. Lee, N. Ayoub, D.K. Agrawal, Mesenchymal stem cells and cutaneous wound healing: novel methods to increase cell delivery and therapeutic efficacy, Stem Cell Res Ther 7 (2016) 37.
[35] R.A. Battaglia, S. Delic, H. Herrmann, N.T. Snider, Vimentin on the move: new developments in cell migration, F1000Res 7 (2018) 1796.
[36] F. Cheng, Y. Shen, P. Mohanasundaram, M. Lindström, J. Ivaska, T. Ny, J.E. Eriksson, Vimentin coordinates fibroblast proliferation and keratinocyte differentiation in wound healing via TGF-β-slug signaling, Proc. Natl. Acad. Sci. U. S. A. 113 (2016) E4320–E4327.
[37] H. Okuyama, B. Krishnamachary, Y.F. Zhou, H. Nagasawa, M. Bosch-Marce, G.L. Semenza, Expression of vascular endothelial growth factor receptor 1 in bone marrow-derived mesenchymal cells is dependent on hypoxia-inducible factor 1, J. Biol. Chem. 281 (2006) 15554–15563.
[38] Z. Zhang, L. Yao, J. Yang, Z. Wang, G. Du, PI3K/Akt and HIF-1 signaling pathway in hypoxia-ischemia (review), Mol. Med. Rep. 18 (2018) 3547–3554.
[39] L. Fan, J. Li, Z. Yu, X. Dang, K. Wang, The hypoxia-inducible factor pathway, prolyl hydroxylase domain protein inhibitors, and their roles in bone repair and regeneration, Biomed. Res. Int. 2014 (2014) 1–11.
[40] S.-C. Hung, R.R. Pochampally, S.-C. Hsu, C. Sanchez, S.-C. Chen, J. Spees, D.J. Prockop, Short-term exposure of multipotent stromal cells to low oxygen increases their expression of CX3CR1 and CXCR4 and their engraftment in vivo, PLoS One 2 (2007) e416.
[41] G.L. Semenza, HIF-1 and mechanisms of hypoxia sensing, Curr. Opin. Cell Biol. 13 (2001) 167–171.
[42] A. Aly, K. Peterson, A. Lerman, L. Lerman, M. Rodriguez-Porcel, Role of oxidative stress in hypoxia preconditioning of cells transplanted to the myocardium: a molecular imaging study, J. Cardiovasc. Surg. 52 (2011) 579–585.
[43] K. Sun, T. Cheng, L. Wu, Y. Hu, J. Zhou, A. Maclennan, Z. Jiang, Y. Gao, W.A. Goddard, Z. Wang, Ultrahigh mass activity for carbon dioxide reduction enabled by gold-iron core-shell nanoparticles, J. Am. Chem. Soc. 139 (2017) 15608–15611.
[44] H.L. Liu, J.H. Wu, J.H. Min, Y.K. Kim, Synthesis of monosized magnetic-optical AuFe alloy nanoparticles, J. Appl. Phys. 103 (2008) 07D529.
[45] C. Sun, J. Lee, M. Zhang, Magnetic nanoparticles in MR imaging and drug delivery, Adv. Drug Deliv. Rev. 60 (2008) 1252–1265.
[46] S. Song, Y. Chong, H. Fu, X. Ning, H. Shen, Z. Zhang, HP-β-CD functionalized Fe3O4/CNPs-based theranostic nanoplatform for pH/NIR responsive drug release and MR/NIRFL imaging-guided synergetic chemo/photothermal therapy of tumor, ACS Appl. Mater. Interfaces 10 (2018) 33867–33878.
[47] A.J. Carlisle, C.A. Lyttle, R.Y. Carlisle, J.M. Maris, CXCR4 expression heterogeneity in neuroblastoma cells due to ligand-independent regulation, Mol. Cancer 8 (2009) 126.
[48] T. Nakayama, N. Mutsuga, G. Tosato, FGF2 posttranscriptionally down-regulates expression of SDF1 in bone marrow stromal cells through FGFR1 IIIc, Blood 109 (2007) 1363–1372.
[49] C. Piard, A. Jeyaram, Y. Liu, J. Caccamese, S.M. Jay, Y. Chen, J. Fisher, 3D printed HUVECs/MSCs cocultures impact cellular interactions and angiogenesis depending on cell-cell distance, Biomaterials 222 (2019) 119423.
[50] E.A. Beierle, L.F. Strande, M.K. Chen, VEGF upregulates Bcl-2 expression and is associated with decreased apoptosis in neuroblastoma cells, J. Pediatr. Surg. 37 (2002) 467–471.
[51] F. Hua, M.G. Cornejo, M.H. Cardone, C.L. Stokes, D.A. Lauffenburger, Effects of Bcl-2 levels on Fas signaling-induced caspase-3 activation: molecular genetic tests of computational model predictions, J. Immunol. 175 (2005) 6235–6237.
[52] J.H. Lee, Y.M. Yoon, S.H. Lee, Hypoxic preconditioning promotes the bioactivities of mesenchymal stem cells via the HIF-1α-GRP78-Akt axis, Int. J. Mol. Sci. 18 (2017) 1320.
[53] A.M. Bader, K. Klose, K. Bieback, D. Korinth, M. Schneider, M. Seifert, Y.-H. Choi, A. Kurtz, V. Falk, C. Stamm, Hypoxic preconditioning increases survival and pro-angiogenic capacity of human cord blood mesenchymal stromal cells in vitro, PLoS One 10 (2015) e0138477.
[54] M. Aragona, S. Dekoninck, S. Rulands, S. Lenglez, G. Mascré, B.D. Simons, C. Blanpain, Defining stem cell dynamics and migration during wound healing in mouse skin epidermis exploring the role of stem cells in cutaneous wound healing, Nat. Commun. 8 (2017) 14684.
[55] S. Saraswati, S.M.W. Marrow, L.A. Watch, P.P. Young, Identification of a pro-angiogenic functional role for FSP1-positive fibroblast subtype in wound healing, Nat. Commun. 10 (2019) 3027.
[56] C. Wiegand, M. Abel, U.C. Hipler, P. Elsner, Effect of non-adhering dressings on promotion of fibroblast proliferation and wound healing in vitro, Sci. Rep. 9 (2019) 4320.
[57] C.H. Lim, Q. Sun, K. Ratti, S. Lee, Y. Zheng, M. Takeo, W. Lee, P. Rabbani, M. Plikus, J. Cain, D. Wang, N. Watkins, S. Millar, M. Taketo, P. Myung, G. Cotsarelis, M. Ito, Hedgehog stimulates hair follicle neogenesis by creating inductive dermis during murine skin wound healing, Nat. Commun. 9 (2018) 4903.
[58] B.-R. Son, L.A. Marquez-Curtis, M. Kucia, M. Wysoczynski, A.R. Turner, J. Ratajczak, M.Z. Ratajczak, A. Janowska-Wieczorek, Migration of bone marrow and cord blood mesenchymal stem cells in vitro is regulated by stromal-derived factor-1-CXCR4 and hepatocyte growth factor-c-met axes and involves matrix metalloproteinases, Stem Cells 24 (2006) 1254–1264.
[59] D. Yang, S. Sun, Z. Wang, P. Zhu, Z. Yang, B. Zhang, Stromal cell-derived factor-1 receptor CXCR4-overexpressing bone marrow mesenchymal stem cells accelerate wound healing by migrating into skin injury areas, Reprogram 15 (2013) 206–215.
[60] R. Salcedo, K. Wasserman, H.A. Young, M.C. Grimm, O.M.Z. Howard, M.R. Anver, H.K. Kleinman, W.J. Murphy, J.J. Oppenheim, Vascular endothelial growth factor and basic fibroblast growth factor induce expression of CXCR4 on human endothelial cells: in vivo neovascularization induced by stromal-derived factor-1alpha, Am. J. Pathol. 154 (1999) 1125–1135.
[61] G.L. Semenza, Expression of hypoxia-inducible factor 1: mechanisms and consequences, Biochem. Pharmacol. 59 (2000) 47–53.
[62] A. Aiuti, I.J. Webb, C. Bleul, T. Springer, J.C. Gutierrez-Ramos, The chemokine SDF-1 is a chemoattractant for human CD34+ hematopoietic progenitor cells and provides a new mechanism to explain the mobilization of CD34+ progenitors to peripheral blood, J. Exp. Med. 185 (1997) 111–120.
[63] T. Schioppa, B. Uranchimeg, A. Saccani, S.K. Biswas, A. Doni, A. Rapisarda, S. Bernasconi, S. Saccani, M. Nebuloni, L. Vago, A. Mantovani, G. Melillo, A. Sica, Regulation of the chemokine receptor CXCR4 by hypoxia, J. Exp. Med. 198 (2003) 1391–1402.
[64] T. Lapidot, O. Kollet, The essential roles of the chemokine SDF-1 and its receptor CXCR4 in human stem cell homing and repopulation of transplanted immune-deficient NOD/SCID and NOD/SCID/B2m(null) mice, Leukemia 16 (2002) 1992–2003.
[65] M. Liu, Q. Li, L. Liang, J. Li, K. Wang, J. Li, M. Lv, N. Chen, H. Song, J. Lee, J. Shi, L. Wang, R. Lal, C. Fan, Real-time visualization of clustering and intracellular transport of gold nanoparticles by correlative imaging, Nat. Commun. 8 (2017) 15646.
[66] C.C. Liang, A.Y. Park, J.L. Guan, In vitro scratch assay: a convenient and inexpensive method for analysis of cell migration in vitro, Nat. Protoc. 2 (2007) 329–333.
[67] T. Gebäck, M.M.P. Schulz, P. Koumoutsakos, M. Detmar, TScratch: a novel and simple software tool for automated analysis of monolayer wound healing assays, Biotechniques 46 (2009) 265–274.